Formation of structural color from lipidic lyotropic liquid crystals

Demo, Šime

University of Split
Faculty of Science

Formation of structural color from lipidic lyotropic liquid crystals

Bachelor thesis

Šime Demo

Split, September 2024.

Temeljna dokumentacijska kartica

Sveučilište u Splitu
Prirodoslovno–matematički fakultet
Odjel za fiziku
Ruđera Boškovića 33, 21000 Split, Hrvatska

Završni rad

Formacija strukturne boje od lipidnih liotropnih tekućih kristala

Šime Demo

Sveučilišni prijediplomski studij Fizika

Sažetak:

Priroda koristi strukturalne boje za kamuflažu, privlačenje i komunikaciju [1]. Unatoč napretku u razumijevanju fotoničkih struktura odgovornih za strukturalne boje, razvojni putevi koji vode do ovih formacija nisu dobro shvaćeni [2]. Kako sustav prelazi iz vezikula u mrežastu strukturu i koja je uloga šećera u tom procesu? Djeluje li samo kao ljepilo ili aktivno djeluje na vezikule, utječući na njihovu organizaciju i funkciju? Ovaj projekt istražuje ta pitanja koristeći lipidne liotropne tekuće kristale za stvaranje takvih struktura. Koristimo model simulacije diskipativne dinamičke čestice (DPD) za predviđanje i dizajniranje bioloških građevnih blokova za strukturalne boje. Tehnika grubog zrna DPD-a omogućuje točne simulacije na većem broju čestica i dužim vremenskim razmacima. Naš model testiran je za prostornu i vremensku konvergenciju, osiguravajući pouzdanost. Vizualizirane putanje jasno otkrivaju različite faze, pružajući uvid u strukturnu evoluciju. Model je također generirao fazne dijagrame za različite lipide, koji mogu igrati ključnu ulogu u strukturalnom bojanju mnogih člankonožaca. Ovaj rad unapređuje naše razumijevanje fotoničkih struktura i otvara put za bio-inspirirano inženjerstvo novih materijala.

Ključne riječi: strukturna boja, lipidni liotropni kristali, DPD

Rad sadrži: 23 stranice, 16 slika, 2 tablice, 24 literaturna navoda. Izvornik je na engleskom jeziku.

Mentor: izv. prof. dr. sc. Damir Kovačić

Neposredni voditelj: dr. sc. Viola Valentina Vogler-Neuling,
dr. sc. Matthias Saba,
Florin Hemmann, mag. phys.

Ocjenjivači: izv. prof. dr. sc. Damir Kovačić,
dr. sc. Viola Valentina Vogler-Neuling,
izv. prof. dr. sc. Larisa Zoranić

Rad prihvaćen: 26. Rujan, 2024.

Rad je pohranjen u Knjižnici Prirodoslovno–matematičkog fakulteta, Sveučilišta u Splitu.

Basic documentation card

University of Split
Faculty of Science
Department of Physics
Ruđera Boškovića 33, 21000 Split, Croatia

Bachelor thesis

Formation of structural color from lipidic lyotropic liquid crystals

Šime Demo

University undergraduate study Physics

Abstract:

Nature employs structural color for purposes such as camouflage, attraction, and communication [1]. Despite progress in understanding the photonic structures responsible for structural color, the developmental pathways leading to these formations are not well understood [2]. How does a system transition from vesicles to a network-like structure, and what role does sugar play in this process? Is it simply a glue, or does it actively interact with vesicles to influence their organization and function? This project explores these questions using lipidic lyotropic liquid crystals to generate such structures. We use a dissipative particle dynamics (DPD) simulation model to predict and design biological building blocks for structural colors. DPD's coarse-graining technique enables accurate simulations over larger particle numbers and longer timescales. Our model was tested for spatial and time convergence, ensuring reliability. Visualized trajectories reveal distinct phases with clarity, providing insight into structural evolution. The model also generated phase diagrams for various lipids, which may play a key role in structural coloration in many arthropods. This work advances our understanding of photonic structures and opens avenues for bio-inspired materials engineering.

Keywords: structural color, lipidic lyotropic liquid crystals, DPD

Thesis consists of: 23 pages, 16 figures, 2 tables, 24 references. Original language: English.

Supervisor: Assoc. Prof. Dr. Damir Kovačić

Leader: Dr. sc. Viola Valentina Vogler-Neuling,
Dr. sc. Matthias Saba,
Florin Hemmann, MSc. Phys.

Reviewers: Assoc. Prof. Dr. Damir Kovačić,
Dr. sc. Viola Valentina Vogler-Neuling,
Assoc. Prof. Dr. Larisa Zoranić

Thesis accepted: September 26th, 2024

Thesis is deposited in the library of the Faculty of Science, University of Split.

Contents

1 Introduction

The thesis serves as a first step toward understanding photonic structure formation in insects. We here give a summary of how these remarkable nanostructures produce color (1.1), and how they might be formed during the developmental stages of the insect (1.1.1 and 1.1.2).

1.1 Structural color

Structural color is a coloration that arises not from pigments or dyes but from nanostructures that interfere with light. This phenomenon, responsible for some of nature's most brilliant displays, occurs through the interaction of light with surfaces or materials that are structured at the nanometer scale. Unlike pigment-based coloration, which relies on the chemical absorption of certain light wavelengths, structural color arises from physical processes like thin-film interference, multilayer reflection, and photonic crystal diffraction. These mechanisms control how light is reflected or transmitted at the nanoscale, with specific wavelengths being amplified or diminished based on the material's internal structure rather than simple scattering. It should be noted that these processes are not wavelength-dependent for non-dispersive materials. [3]

This coloration can be found across various species in nature, such as in the iridescent wings of butterflies and moths (Figure 1 A), feathers of birds like peacocks (Figure 1 B) or iridescent scales of beetles (Figure 1 C). These structures are highly efficient at producing vivid, generally angle-dependent colors, often with a degree of durability and resistance to fading that surpasses that of pigments.

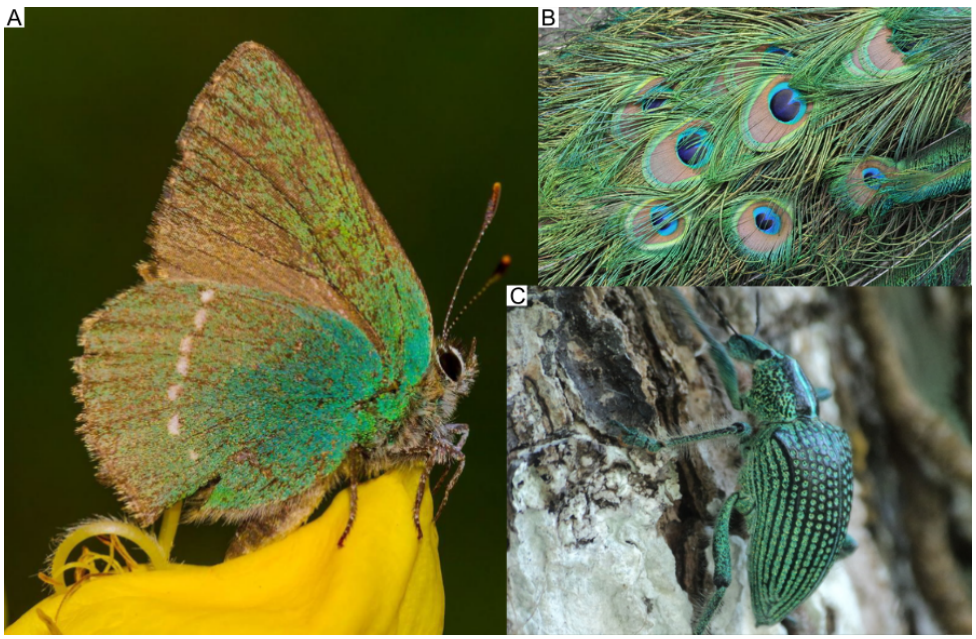

Figure 1: *Examples of structural coloration in nature. A: Callophrys rubi B: Pavo cristatus [4] C: Entimus imperialis [5]*

1.1.1 Photonic crystals

Photonic crystals are highly ordered, periodic structures that can control the propagation of light. They are characterized by a periodic variation in the refractive index, much like the periodic arrangement of atoms in a solid crystal affects the movement of electrons. Photonic crystals give rise to frequency-dependent light propagation properties even though they are composites made of non-dispersive constituent materials. Similar to their electronic counterparts, they even lead to frequency ranges with vanishing density of states, also known as photonic band gaps. A photonic band gap is a range of wavelengths where light cannot propagate within the material. This makes them particularly useful for manipulating light. Photonic crystals derive their optical properties from interference based on two essential characteristics:

a) Refractive index contrast: a significant difference in refractive index between two constituent materials that form the periodic structure.
b) Periodicity: the spacing of the periodic structure is in the same order as the wavelength of the light that is to be manipulated, typically in the visible spectrum for natural systems.

When light enters a photonic crystal, it undergoes multiple scattering events at the boundaries between the regions of different refractive indices. As a result, certain wavelengths experience constructive interference, while others experience destructive interference. The outcome is a highly selective reflection of specific wavelengths of light, creating brilliant structural color.

Photonic crystals are classified based on the dimensionality of their periodic structures in three different classes: 1D, 2D, and 3D photonic crystals. 1D photonic crystals are of the simplest form, consisting of alternating layers of high and low refractive index materials. In nature, they're found in reflective layers of certain beetles' scales. In 2D photonic crystals, the structure extends in two directions, often forming hexagonal or square lattice patterns. These are commonly found in butterfly and moth wings, contributing to their vivid coloration. 3D photonic crystals are the most complex and create a fully three-dimensional periodic arrangement of refractive index variation.

1.1.2 Gyroids

Gyroids represent one of the most fascinating three-dimensional structures that appear in nature as photonic crystals. It is a type of minimal surface, meaning that it has zero mean curvature, making it an incredibly efficient and stable structure. Gyroids are not composed of straight lines or planes but consist of a smooth, triply periodic minimal surface that extends in all three dimensions. While the surface itself is continuous, it has an associated skeletal graph or network that represents its underlying symmetry and structure. Gyroids can also approximate constant mean curvature surfaces, often described through nodal (or level) surfaces in mathematical

models [6]. The gyroid structure is a triply periodic minimal surface (TPMS), kind of periodic implicit surface with zero mean curvature, that is, the surfaces that locally minimize surface area for a given boundary. The TPMS is composed of infinite, non-self-intersecting, periodic surfaces in three principal directions. It has to be mentioned that other TPMS are also made by insects and produce equally vibrant colors [7]. Gyroids are mainly characterized by:

- No planar symmetry: Unlike other simpler photonic crystals like opals or cubic structures, gyroids are chiral structures, leading to complex patterns of light reflection and refraction [8]
- High surface area: due to the minimal surface nature, gyroids have a large surface area, which maximizes interaction with light
- Interwoven networks: The gyroid structure is composed of two interpenetrating but non-intersecting networks

When light enters a gyroid-based photonic crystal, the light waves bounce around the complex labyrinth of surfaces. The structure's geometry ensures that certain wavelengths of light interfere destructively, leading to the formation of a photonic band gap. The wavelengths that do not fall within this band gap are reflected, which gives rise to the structural colors observed in nature. One such occurrence is found in the scales of *Callophrys rubi* (see Figure 2) [9]. Scales contain gyroid structures that reflect mostly green light, giving the butterfly its iridescent color. The gyroids within the scales form a photonic crystal that selectively reflects green wavelengths due to their interaction with visible light, while other wavelengths pass through or are absorbed.

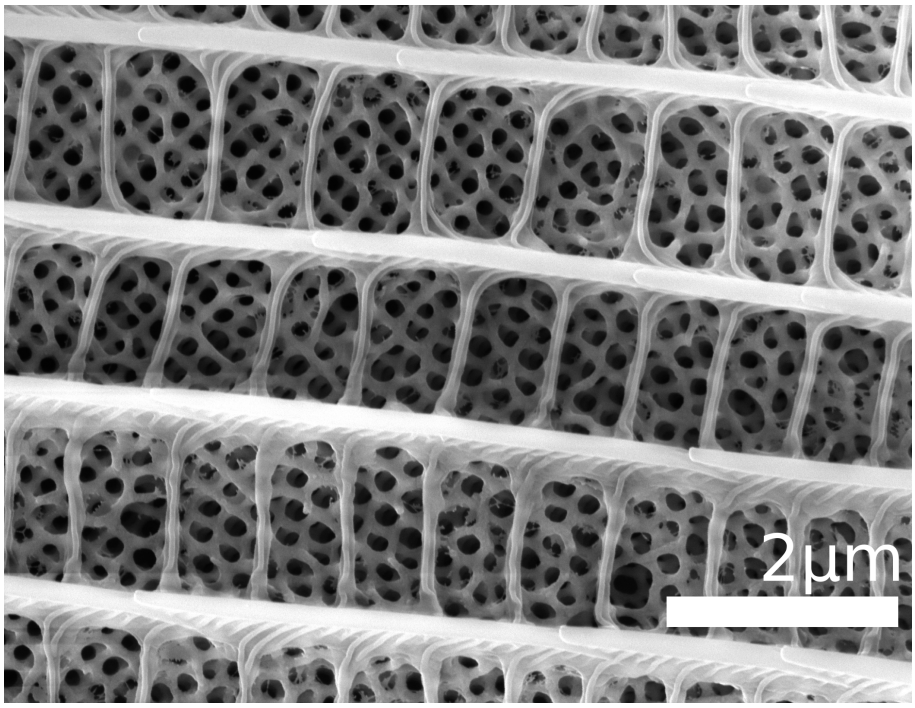

Figure 2: *Periodic gyroid structure responsible for structural coloration of C. rubi wings*

1.2 Lipidic lyotropic liquid crystals

Lipids are a group of organic compounds that include fats, waxes, fat-soluble vitamins, phospholipids, monoglycerides, and others [10]. Their main functions are storing energy, acting as structural cell components, and signaling. One of their key characteristics is their amphiphilic nature, meaning they contain both hydrophilic (water-loving) and hydrophobic (water-repelling) regions within the same molecule. A typical lipid structure consists of a hydrophilic head and a hydrophobic tail. The hydrophilic head consists of a polar functional group, such as the phosphate group in the case of phospholipids. This head interacts favorably with water and other polar molecules. The hydrophobic tail is a nonpolar part of the molecule, consisting mainly of a long hydrocarbon chain. These tails tend to avoid contact with water and prefer to be in the proximity of other hydrophobic substances.

Lipidic lyotropic liquid crystals (LLCs) are a class of materials that form when certain lipids interact with a solvent (mostly water) and self-assemble into ordered yet fluid, structures. By breaking down their name we can gain further insight into the nature of LLCs. The term lipidic refers to their building material, lipids. The terms "lyo" and "tropic" mean "dissolve" and "change", respectively. Lyotropic would then refer to the fact that these liquid crystalline phases form in response to the addition of solvent. Lastly, "liquid crystals", describe their ability to flow like a liquid while maintaining a degree of molecular order, akin to a crystal. LLCs typically have very diverse phase diagrams. This is a consequence of their amphiphilic nature. Under certain conditions such as water concentration, temperature, and pH, they form a wide variety of structures. These geometries can include more simple phases such as micellar phases, vesicles, and bilayers, and more complex phases like gyroids or networks. It is important to note that the gyroid can in principle be formed as a bilayer, but hydrophobic tails can also form a network domain which is the volume enclosed by the orientable gyroid surface. Nature employs these phases for various tasks, bilayers for membranes of cells and organelle, vesicles for transport of molecules within the cell, secretory vesicles involved in the exocytosis of neurotransmitters, and other such substances.

1.3 Hypothesis

The processes behind the formation of structures responsible for structural color in nature remain unknown and are yet to be fully understood. There are some hypotheses of chitin polymerization but are yet to be proven by *in vivo* imaging [11].

Monoolein (MO) and oleic acid (OA), both found in biological systems, when combined in the right conditions, form different phases [12]. We begin with a simple solution of MO, OA, and water. At a high enough concentration of OA in MO and a slightly basic environment, it has been shown experimentally that vesicles occur (see Figure 3). We hypothesize that upon

introducing sugar such as chitosan to the system consisting of large vesicles, it glues them together. Over a long enough period of time (up to several weeks), the length scale of a system reduces, and vesicles together with chitosan rearrange themselves into a gyroid.

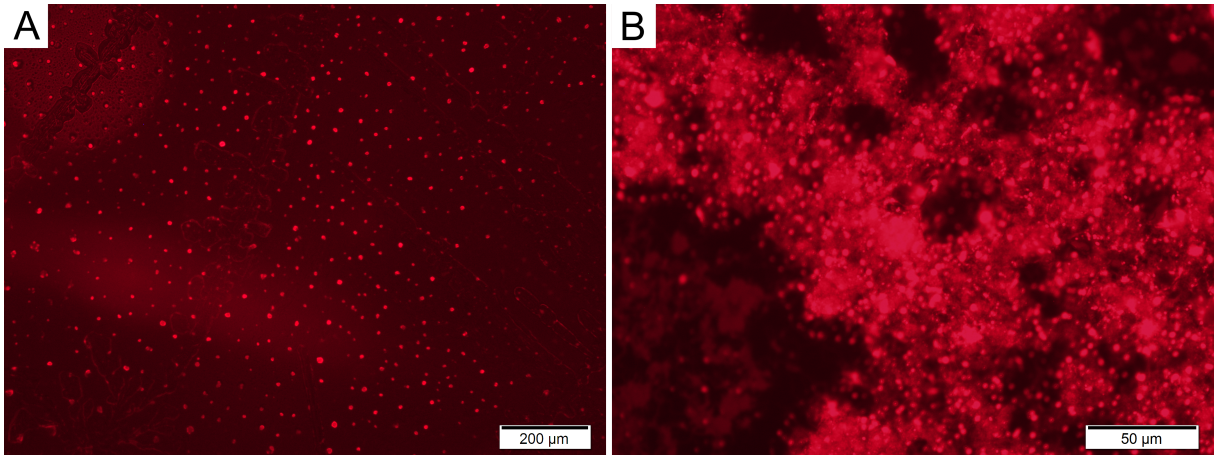

Figure 3: *Preliminary experimental results of 50 % Oleic Acid and 50 % Monoolein solution after vesicle extrusion. The dye used is Nile Blue A and images are taken of a dried sample. Image A shows a system with no chitosan. Image B shows a system with 0.5 % chitosan.*

Chitosan's interaction with vesicles has been proven experimentally by measuring their hydrodynamic radius before and after the introduction of chitosan. Some of our preliminary experimental observations have shown system shrinking and network-like structures being formed (Figure 3 B).

We seek to understand how exactly does chitosan interact with the system and how does the length scale change when the system goes from vesicles to a gyroid. As a first step towards this goal, this thesis employs dissipative particle dynamics simulation (DPD) (2.1) to model the phase diagram of oleic acid in water. It therefore contributes to a theoretical understanding of the necessary circumstances for vesicle formation and builds the basis for simulating the hypothesized phase transition to the gyroid phase.

2 Methods and theory

To prove the stated hypothesis, we used computational simulations (2.1) built upon several different theories (2.2 and 2.4.1) in order to simulate the behavior of our solutions accurately.

2.1 Molecular dynamics and dissipative particle dynamics

Molecular dynamics (MD) is a computational simulation technique used to study the physical movements of atoms and molecules over time. It can be used to model how atoms interact, move, and evolve under various conditions. It can give insight into different biomolecular functions, membrane dynamics, and material properties at an atomic scale. It follows a very simple algorithm:

(1) collection of positions and velocities of every atom

(2) calculating forces and energies between atoms typically via classical force fields that emulate covalent, electrostatic, and van der Waals interactions or employing forces such as Langevin force

(3) applying an iterative time-integration algorithm to compute the phase space at discrete time steps from a starting configuration

When dealing with a large number of molecules on a long enough time scale, MD gets very computationally expensive [13]. DPD employs a coarse-grained model of the molecules and simple effective short-range potentials to mitigate computational limitations. Developed by Groot and Warren back in 1997 [14], the method has proven itself to be extremely useful for simulating systems on a mesoscopic scale. It requires less computational resources and is favorable for systems with large particle counts as well as long time scales.

The total force between two DPD particles is given by a sum of three governing forces in a DPD simulation, conservative (2.1), random (2.2), and dissipative force (2.3). In a system of N particles of equal mass M, positions $\vec{r}_i$ and velocities $\vec{v}_i$, forces are defined as follows:

$$\vec{F}_{ij}^{C} = \begin{cases} a_{ij}\omega^{D}\hat{r}_{ij}, & |\vec{r}_{ij}| < r_c \\ 0, & |\vec{r}_{ij}| \geq r_c \end{cases} \tag{2.1}$$

$$\vec{F}_{ij}^{R} = \begin{cases} \vec{F}_{ij}^{R} = \sigma\omega^{R}(|\vec{r}_{ij}|)\zeta_{ij}\hat{r}_{ij}, & |\vec{r}_{ij}| < r_c \\ 0, & |\vec{r}_{ij}| \geq r_c \end{cases} \tag{2.2}$$

$$\vec{F}_{ij}^{D} = \begin{cases} \vec{F}_{ij}^{D} = -\gamma\omega^{D}(|\vec{r}_{ij}|)(\hat{r}_{ij} \cdot \vec{v}_{ij})\hat{r}_{ij}, & |\vec{r}_{ij}| < r_c \\ 0, & |\vec{r}_{ij}| \geq r_c \end{cases} \tag{2.3}$$

where $\vec{r}_{ij} = \vec{r}_i - \vec{r}_j$, $\vec{r}_{ij} = |\vec{r}_{ij}|\hat{r}_{ij}$, and $\vec{v}_{ij} = \vec{v}_i - \vec{v}_j$. Conservative force (2.1) drives particles toward their equilibrium positions. Random force (2.2) introduces noise into the system, mimicking thermal fluctuations. Dissipative force (2.3) acts as a thermostat, controlling the temperature of the system. The variables γ and σ determine the strength of dissipative and random forces, respectively. ζ_{ij} is a symmetric Gaussian random variable with zero mean and unit variance. It is a statistically independent random variable for each particle pair and time step that follows a zero mean, unit variance Gaussian probability distribution. And finally, ω^D and ω^R are weight functions of their respective forces.

All forces act within a sphere of interaction radius r_c, which is the length scale of the system, as it can be seen in equation (2.1). a_{ij} is the interaction parameter between two particles and since conservative force is a repulsion force, it is always positive. Its calculation and physical meaning will be detailly discussed in the following sections. ω^D and ω^R are both r_c dependant functions and are related as:

$$\omega^D = (\omega^R)^2 = \begin{cases} 1 - \frac{|\vec{r}_{ij}|}{r_c}, & |\vec{r}_{ij}| \leq r_c \\ 0, & |\vec{r}_{ij}| > r_c \end{cases} \tag{2.4}$$

Strengths γ and σ of the forces are dependent on energy of the system and due to the fluctuation-dissipation theorem are related as:

$$\sigma^2 = 2\gamma k_B T. \tag{2.5}$$

The integration algorithm employed by a DPD simulation is the velocity Verlet (VV) algorithm [15]. Unlike the Euler algorithm, VV is a leapfrog method that updates positions and velocities in a staggered manner, providing stability and more importantly errors are second order instead of first.

2.2 Group contribution theory

Interaction parameter a_{ij} in equation (2.1) can be calculated in a few different ways, fragment molecular orbital method, group contribution theory, Monte-Carlo simulations, and lately even machine learning [16, 17]. My method of choice is the group contribution method. It is relatively simple to implement in a short amount of time and offers great insight into molecular properties such as the contribution of different groups to cohesive energy or molar volume [18]. Theory estimates thermodynamic and physical properties of chemical compounds based on the contributions of functional groups within their molecular structure. The core idea behind group contribution theory is that the properties of any molecule can be approximated as the sum of contributions from simpler structural groups. These groups could include functional groups like hydroxyl or methyl groups or even specific atom types. Theory is driven by three key assumptions:

(1) property of a compound is the sum of contributions from all its functional groups

(2) the contribution of a functional group is assumed to be nearly the same in different molecules

(3) each group's contribution is assumed to be independent of the surrounding molecular environment while small corrections are allowed

These assumptions allow a modular and systematic approach to predicting the properties of different molecules.

2.3 Flory-Huggins theory

Since we will be dealing with polymer-polymer and polymer-solvent mixtures we needed an approach that can handle mixing species of not necessarily two equal volumes. A theory that can solve those problems is the Flory-Huggins theory. The Flory-Huggins theory is a lattice model, allowing it to accommodate the unique characteristics of polymers, such as large size and chain-like structures [19]. In the Flory-Huggins framework, each lattice site is occupied by a solvent molecule or a segment of a polymer chain. Polymers with their above average size tend to occupy more sites than water molecules for example. This leads to a smaller entropy of mixing since we are dealing with fewer possible configurations.

At the heart of Flory-Huggins theory are really only two equations, one which relates *Flory-Huggins parameter* χ_{ij} and free energy of mixing F_{mix} and one which relates χ_{ij} to mixing energies u_{ij}.

$$F_{\text{mix}} = RT\left[\frac{\phi_1}{N_1} ln\phi_1 + \frac{\phi_2}{N_2} ln\phi_2 + \chi_{12}\phi_1\phi_2\right] \tag{2.6}$$

$$\chi_{12} = \frac{z}{2}\frac{2u_{12} - u_{11} - u_{22}}{k_B T} \tag{2.7}$$

In equation (2.6) ϕ_1 and ϕ_2 are the volume fractions of the solvent and polymer, respectively. N_1 and N_2 are the degrees of polymerization of the solvent and polymer and finally $\chi\phi_1\phi_2$ is the enthalpic term. This term accounts for interactions between different species. In equation 2.7 z is a coordination number. Since we are considering a simple cubic lattice it would be $z = 3$. From equation (2.6) we can conclude that higher χ means higher F_{mix} which results in unfavorable mixing because the required energy for mixing is so high. While higher mixing energy u_{ij} does mean higher interaction parameter a_{ij}, the two are not the same. Mixing energies measure energy change upon two polymers mixing while interaction parameters determine the strength of repulsive and attractive forces between the particles.

2.4 Methodology

2.4.1 Calculating the interaction parameter

In order to simulate the behavior of molecules of interest accurately, we need an interaction parameter a_{ij}. Groot and Warren have calculated relationship between a_{ij} and χ_{ij}

$$a_{ij} = a_{ii} + 3.268\chi_{ij}. \tag{2.8}$$

As shown by Rubinstein, the Flory-Huggins parameter can be expressed in terms of Hildebrands solubility parameters

$$\chi_{ij} = \frac{V_{\text{segment}} \left(\delta_i - \delta_j\right)^2}{RT}. \tag{2.9}$$

Hildebrands solubility parameter δ is particularly useful because it is related to group contribution theory and is calculated within this framework via:

$$\delta = \sqrt{\frac{E_{\text{cohesive}}}{V_{\text{pm}}}}, \tag{2.10}$$

where E_{cohesive} and V_{pm} are group contributions to cohesive energy and partial molar volume, respectively. It provides a numerical estimate of the degree of interaction between materials and is a good indication of solubility. The only drawback is poor estimation for polar materials, but works really well for nonpolar ones, such as polymers. From equation (2.9) we can see that materials with similar solubility parameters are likely to be miscible.

This thesis aimed to replicate the published result, but upon a closer look, it served as an inspiration too. [21]. The authors have coarse-grained OA into 4 beads, $H1 - T1 - T2 - T1$. After taking a closer look at the structure of OA, the only way to do this is if we split it into three different groups (see Figure 4).

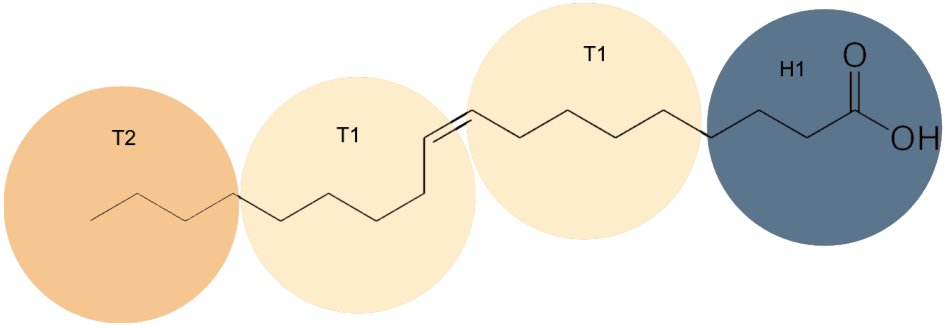

Figure 4: *Visualized representation of coarse-graining the oleic acid into three different types of beads, H1, T1, and T2.*

In order to keep the volumes of the beads similar, we conclude that a water bead has to have four water molecules in it (see Figure 5).

	E_{cohesive} / J mol^{-1}	V / cm^3 mol^{-1}
$-COOH$	27630	28.5
$-CH_2-$	4940	16.1
$=CH-$	4310	13.5
$-CH_3$	4710	33.5
H_2O	18000	18

Table 1: *Group contributions to cohesive energy and molar volume from FEDORS database.*

	$H1$	$T1$	$T2$	W
δ	23.51	17.58	15.45	31.62

Table 2: *Hildebrands solubility parameter calculated with data from Table 1*

.

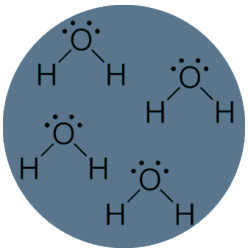

Figure 5: *Visualized representation of a water bead containing four molecules of water.*

Using data from Table 1 [20], we calculate Hildebrands solubility parameters for our beads. Note that some contributions to molar volume can be negative. It suggests that that particular group, when added to a molecule leads to a more compact structure. It allows surrounding atoms or groups to pack more closely than they would in the absence of this group.

Together with data from Table 2 and 1, we can create an interaction parameter matrix (see Figure 7). While interaction parameters from the literature and from our results are similar, they are not exactly the same. This is due to not knowing the exact method used to obtain said parameters in the literature. Also, if we take a closer look, the main differences are in polymer-solvent interactions. As previously stated, group contribution theory is known to lack accuracy in those types of interactions.

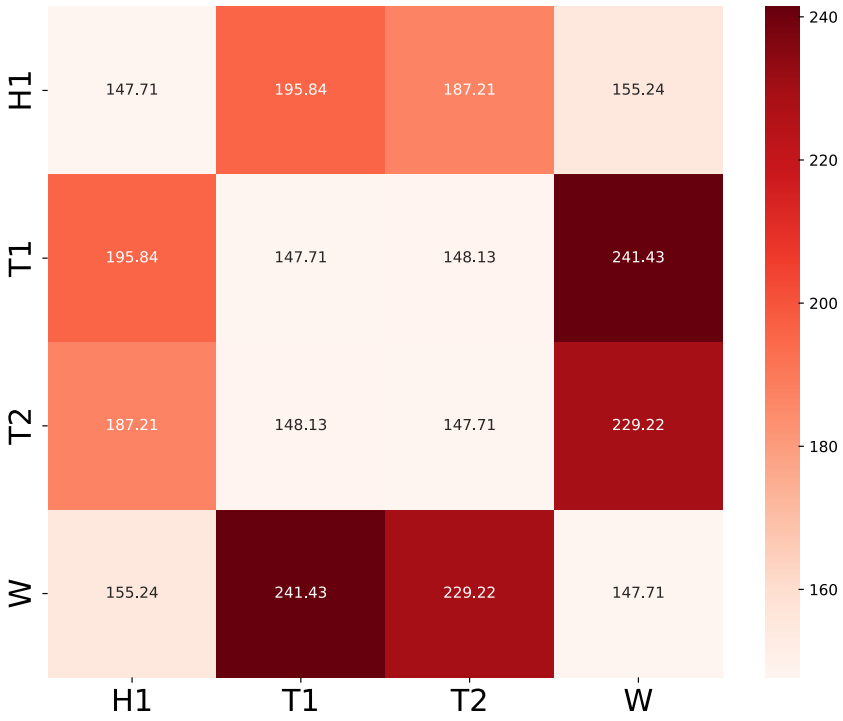

Figure 6: *Interaction parameter matrix [21].*

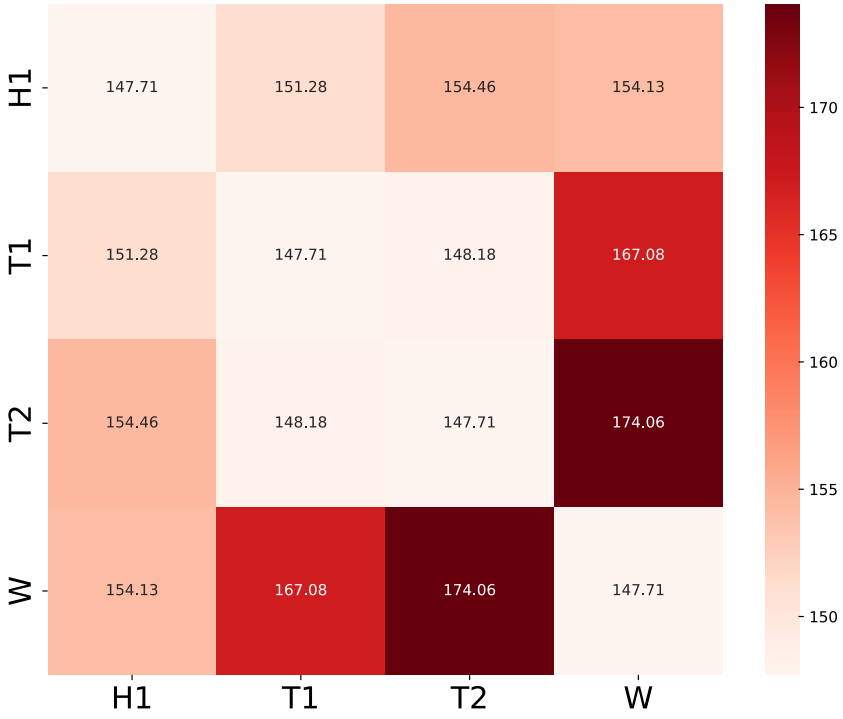

Figure 7: *Interaction parameter matrix calculated by the theory introduced here (equations* (2.8), (2.9), (2.10)*)*

.

3 Results and discussion

3.1 Replication of oleic acid solution phase diagram

The first step is the replication of the oleic acid phase diagram [21]. This served as an introduction to DPD for us and has uncovered some other problems that come with simulation work. Since we wanted to be positive that our simulation works as intended, we mostly used parameters used by the published paper. Used software was not mentioned so we settled on DL_MESO, written in C++ and Fortran and developed specifically for mesoscale simulations [23]. We ran 80 simulations, with a simulation box length of 15.9 su (simulation units) with periodic boundaries, interaction parameters from interaction matrix from Figure 6, $r_c = 1$. Spring force connecting the nearest neighbour beads is given by $\vec{F}_{ij}^{S} = -k_S\left(|\vec{r}_{ij}| - r_S\right)\hat{n}_{ij}$ where $k_S = 100\frac{k_B T}{r_c^2}$. Equilibrium bond length in literature is usually set to 86% of r_c, hence $r_S = 0.86 r_c$. The noise parameter σ and the friction parameter γ are set to 3.0 and 4.5, respectively. Groot and Warren have shown that for a number density ρ, or rather a number of particles in a unit volume, 3 is a reasonable choice. Increasing it provides no measurable gain in accuracy and since calculation time is proportional to ρ^2, it increased drastically. The timestep has been conservatively set to 0.03. By taking a look at how temperature deviates from the set value, one can increase the timestep until the variance isn't bigger than 2-3%. Number of steps chosen was rather large to allow all of the phases to reach its equilibrium state. I chose 300000. The boundary halo, responsible for copying particle data in the neighboring domain or across periodic boundaries, has been set to $2r_c$. Since the particle number and volume of the system don't change and the temperature fluctuates around a mean value, the chosen ensemble has been a canonical ensemble.

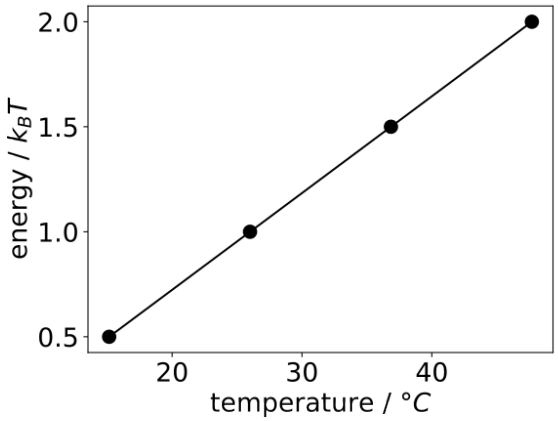

Figure 8: *Linear relation of temperature in real-world units with respect to simulation units; T=21.7T_{su}°C + 4.3°C*

The reason why simulation units are even used comes down to computational efficiency and the physical complexity of physical interactions at different scales. Simply put, it is much more efficient for computer to use scaled and dimensionless units and for human to do conversion

afterwards. To convert simulation units to real-world values, one has to look at some real-world values and map simulation results onto those values. When comparing the thickness of the bilayer in our simulations and comparing them to real-world measurements, we get that $r_c \approx 1$ nm [22]. To get the temperature in Celsius or Kelvin, one can look at the melting point and vesicle disruption temperatures of oleic acid. Using data from the original paper we've calculated values seen in Figure 8.

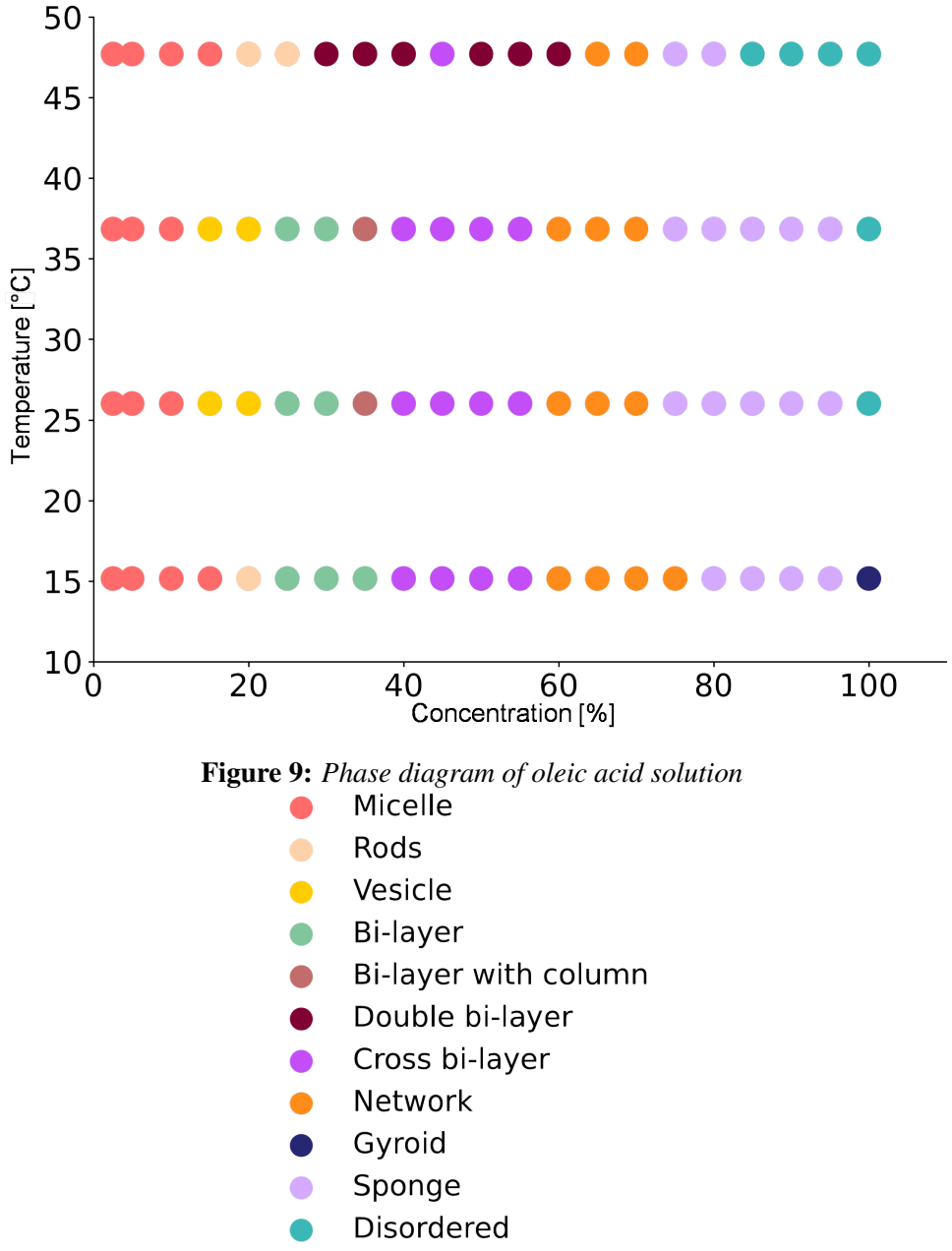

Figure 9: *Phase diagram of oleic acid solution*

The phase diagram has been replicated to a large degree, with some minor additions (see Figure 9). Up to 15 % concentration, regardless of the temperature, we only see micelles, which tend to group into a larger one at higher temperatures. Around 20 %, at low and high temperatures we see cylindrical micelles which have not been reported in the original paper, while at medium temperatures we start seeing the vesicle phase form together with a micelle in the same simulation box. Increasing the concentration promotes bilayer formation and at

35 % at medium temperatures and high temperatures, we start seeing bilayer with column and double bilayer, respectively. Between 40% and 55% the cross bilayer dominates, only at the high temperature does the double bilayer occur. Between 60 % and 75 % network phase starts forming across the whole temperature range and the same goes for the sponge phase at concentrations between 80 % and 95 %, with some disordered phases at the highest temperature. For 100 % of oleic acid, the gyroid forms at low temperatures, while anything higher than around 15^{o}C turns into a disordered phase, although, the resolution of the phase diagram in that region should be increased.

Successful replication serves as proof that our model does work, and that the lipid being simulated is oleic acid and not a random mush of atoms.

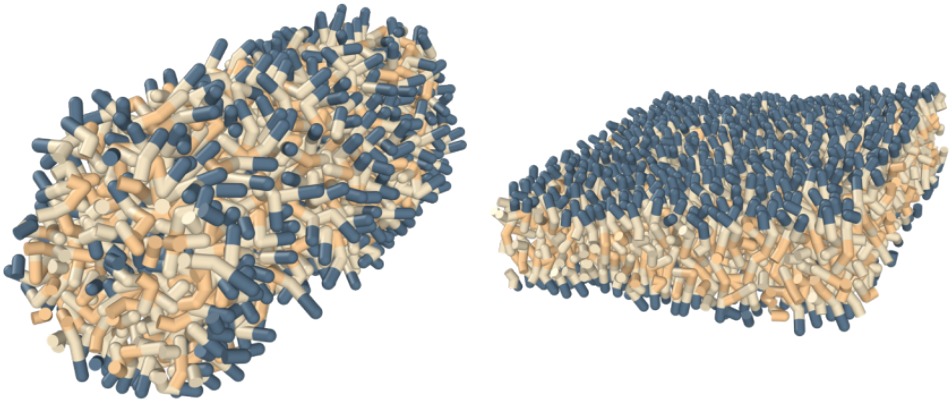

Figure 10: *Visualized trajectories; cylindrical micelle/rod on the left, bilayer on the right.*

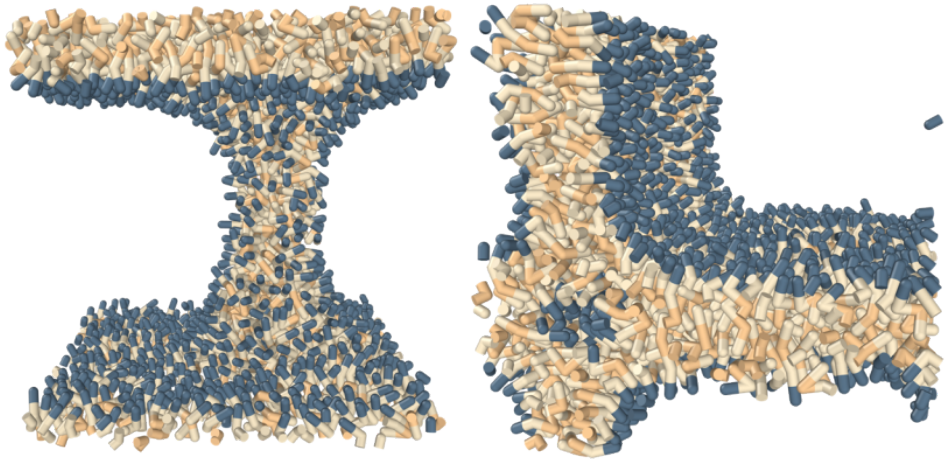

Figure 11: *Visualized trajectories; bilayer with a column on the left, cross bilayer on the right.*

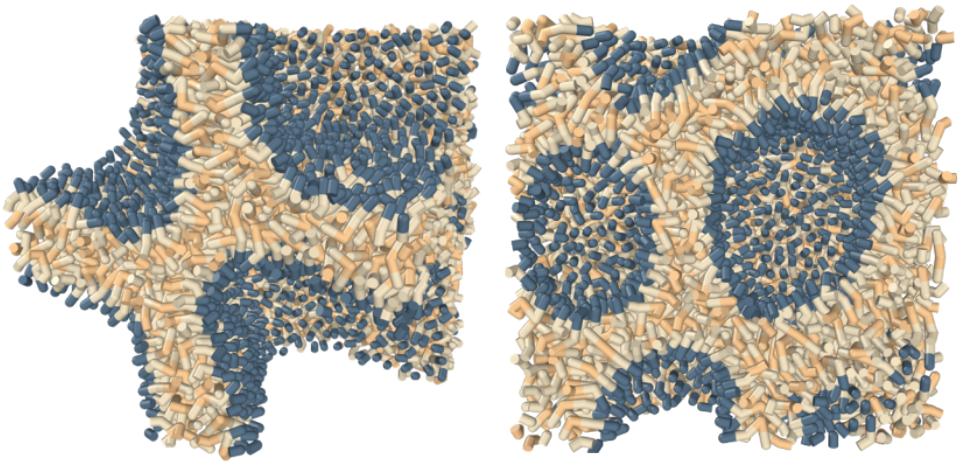

Figure 12: *Visualized trajectories; network on the left, sponge on the right.*

3.2 Convergence testing

In order to proceed with our work, we first need to test the convergence model, both temporal and spatial. Temporal convergence ensures that the simulated system is in a stable state and that simulation artifacts are minimal while ensuring physical realism. Decreasing or increasing system size at some point shouldn't provide a different simulation result. At that same point, no significant simulation or periodic boundary artifacts should be found. Finding this point is exactly the purpose of spatial convergence.

3.2.1 Temporal convergence

To see if the system converges in time or not, we've carried out a cross-correlation analysis. In order to decrease the amount of noise in the images being correlated, instead of taking snapshots of the whole simulation box, we took only the densities of hydrophilic heads. Since our simulation box is split into voxels because of the specific parallelization approach, we had to combine all of those voxels into a (in this case) 65x65x65 matrix (Figure 13).

Since that is a pretty large piece of data, we also decided to reduce the resolution to the point where it is significantly smaller but still maintains all the information. We reduced it down to a 13x13x13 matrix. Then we proceeded to correlate all of the timesteps to the last timestep, where we hopefully have a phase formed. Correlation was conducted with SciPy's *correlate* function, which uses Fast Fourier Transform (FFT) in order to perform the correlation more quickly [24].

In Figure 14 we can see that convergence isn't perfect but it does increase drastically. Fluctuations near the end are the results of the random force employed by the DPD algorithm. Spikes in correlation where the phase hasn't been formed yet occur most likely because of the similarity of the two phases we can see here, bilayer with column and bilayer in the end.

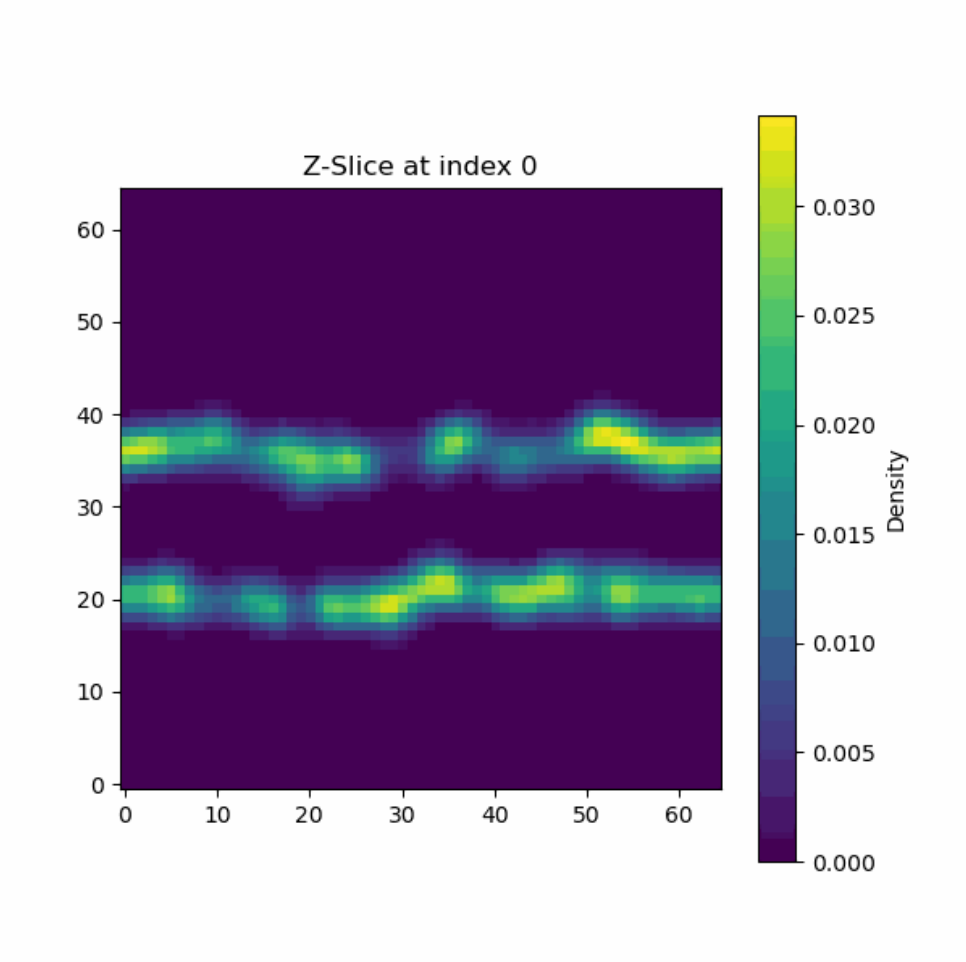

Figure 13: *Slice of a bilayer density map at 0th index.*

One might say that this isn't a good enough method and metric, which is not entirely wrong, but we leave that for the outlook. Before trying image analysis, we tried pressure tensor analysis. Pressure tensor is stress tensor over volume. We've monitored all of the pressure tensor components over time and we haven't seen any useful data. This was to be expected since our phases, while having crystalline structure, are still liquid.

3.2.2 Spatial convergence

Spatial convergence has already been conducted by the original authors. They report exponential dependency of concentration required for bilayer and bilayer with column phase to be formed with respect to the simulation box size. Mentions of other phases have not been presented nor did the reasoning behind this dependency.

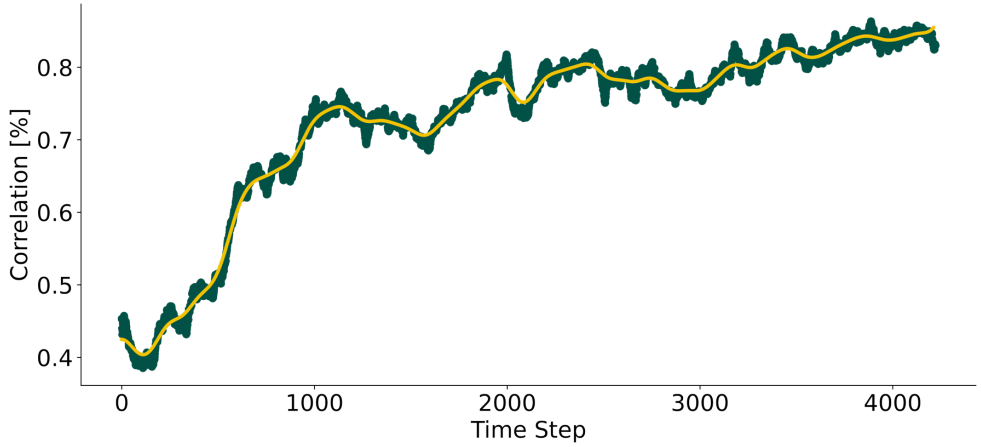

Figure 14: *Correlation plotted as a function of time step; yellow line indicating Gaussian filter applied on original data in green. The plot shows correlation steadily increasing in the first couple thousand steps after which the rate of correlation increase goes down. This shows signs of convergence, but an imperfect one.*

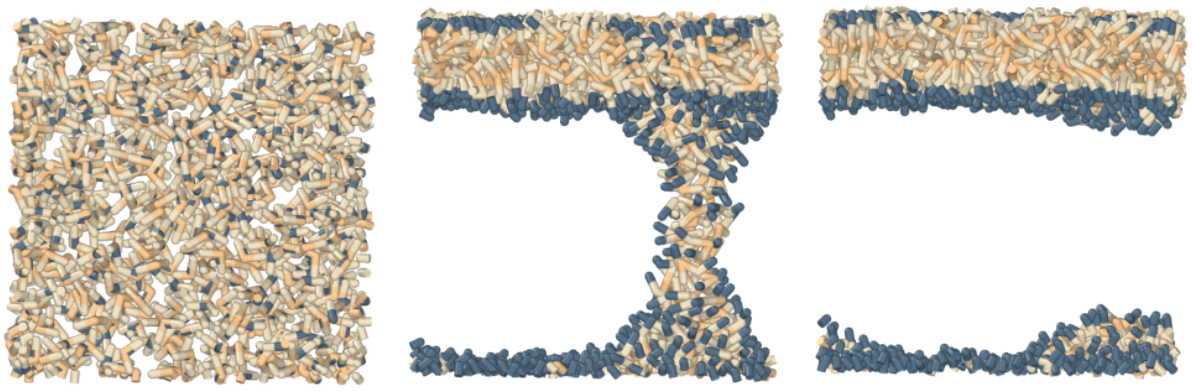

Figure 15: *Visualized trajectories used for Figure 14; Left most image taken at time step 0, middle one at time step 2000 and right one at time step 4000.*

3.3 Phase identification

During the creation of the phase diagram, it has been apparent that manually looking at visualized trajectories of different phases is not the best way to identify them. It is slow and in some more complex phases, inaccurate.

In order to solve this problem, I have developed a lipid vector direction analysis. I take a vector from the last bead in the lipid chain to the very first one, the hydrophilic one. We project it onto the plane and measure its angle against one of the axes. This has proven to work great for less complex phases. That includes all of the phases below 60% concentration on the phase diagram.

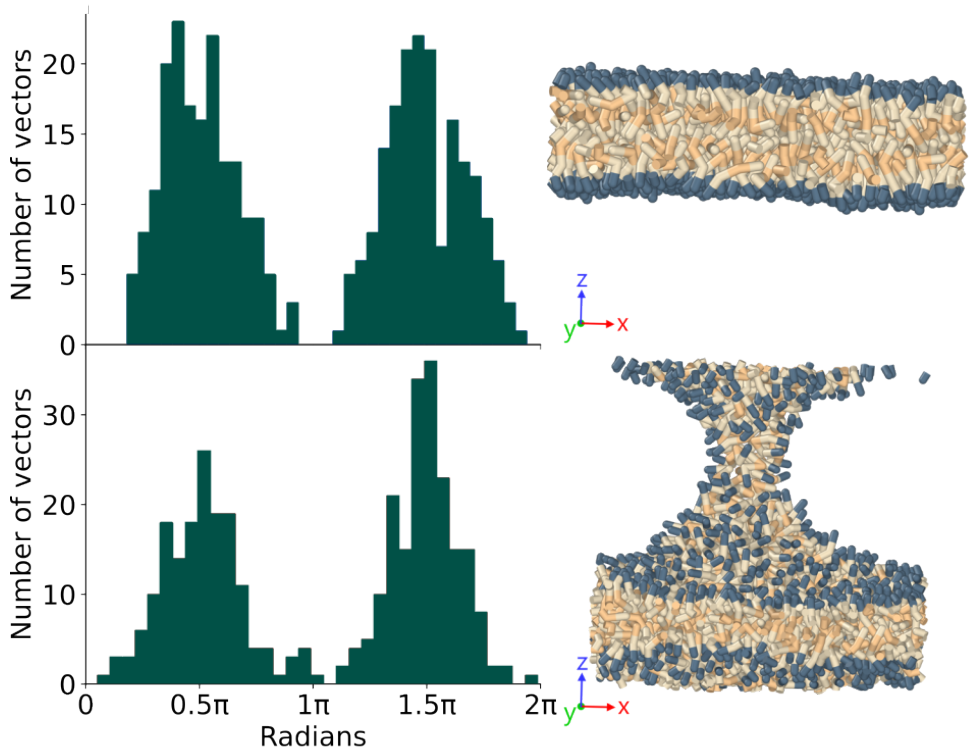

Figure 16: *Vector direction analysis example: bilayer (upper graph and image) vs bilayer with column (bottom graph and image).*

The bilayer phase (see Figure 16), shows two peaks and no data points near π and 2π radians. On the bilayer with column phase, We still see two peaks indicating a bilayer, but we can also see a number of data points around π and 2π radians, indicating lipids oriented perpendicularly to ones forming a bilayer.

4 Conclusion and outlook

By seeking to unravel the processes behind the formation of nanostructures responsible for structural color in nature I've developed some new ideas and simulations which pave the way forward to further understanding of structural color.

Script for calculating solubility, Flory-Huggins χ, and interaction parameters have been developed. Solubility outputs match one-for-one when compared to software like J-OCTA. Flory-Huggins and interaction parameters are accurate as well, until water beads are introduced. Lipid-lipid (and lipid-sugar) interactions are therefore accurate while lipid-water (and sugar-water) interactions are less accurate. While we know what interaction parameters look like in literature, we don't know what method was used to obtain them. The level of accuracy can be tested if more simulations are conducted while using parameters calculated by our script.

Using the original interaction parameters, the phase diagram has been successfully replicated with even some additional phases reported. All simulation results have been verified for temporal convergence by us, and some spatial convergence testing has been done by original authors. Further improvements to the phase diagram and even experimental testing can be made. For each temperature, we've ran simulations for 20 different concentrations, just like the original authors. To gain more insight and prepare data for experimental measurements, one could do the same for a few concentration data points. Concentrations of biggest interest would be concentrations where vesicles are found. This part of the theoretical phase diagram both in literature and in this thesis is extremely blurry. The second most interesting concentration would be concentration where there are the most phases. Such concentrations would be around 20 % and around 40 % where we can see up to 5 different phases occurring along the whole temperature range. Just even to get an idea of where phase transition occurs would be beneficiary for experimental testing.

The phase identification process has been made faster and more reliable through a vector direction analysis script developed by us. It is easily useable and highly accurate for phases that occur under 60% concentration on our OA solution phase diagram.

To get vesicles as large as the ones measured in experiments (300-500 nm in diameter) we would have to increase the system size. Simulations that yielded results for the phase diagram had a simulation box length of only 16 nm. To get vesicles comparable to ones in experiments, the simulation box length would have to be at least 400-600 nm. The maximum box length achieved by us has been 100 nm. The limiting factor was time. While our workstation had enough memory, it didn't have enough CPU power to finish the simulation in a reasonable amount of time. This is why we've turned to high-power computing (HPC). Supercomputer access proposal has been written and required data such as memory usage has been measured.

After getting enough computing power and accurate interaction parameters for lipid-water

or sugar-water interactions, one should have no problem introducing chitosan into a stable vesicle system and observing its behavior. This could potentially solve the puzzle of how exactly are gyroids found in certain butterfly species. Given the lack of experimental oleic acid phase diagrams in the literature, conducting experimental testing while following guidelines of provided theoretical oleic acid could provide valuable insights into oleic acid behavior and fill this gap in the literature.

5 Bibliography

[1] V. V. Vogler-Neuling et al.: *Biopolymer Photonics: From Nature to Nanotechnology*, Advanced Functional Materials, 34, 35, 2306528, 2024.

[2] Sun J. et al.: *Structural coloration in nature*, RCS Adv., 3, 14862-14889, 2013.

[3] S Kinoshita, S Yoshioka and J Miyazaki: *Physics of structural colors*, Reports on Progress in Physics, 71, 076401, 2008.

[4] Stefano: Pavo cristatus, iNaturalist https://inaturalist.ca/photos/407408152 licensed under CC BY-NC-SA 4.0 https://creativecommons.org/licenses/by-nc-sa/4.0/

[5] André Menegotto: Entimus imperialis, iNaturalist https://inaturalist.ca/photos/13178720 licensed under CC BY-NC-SA 4.0 https://creativecommons.org/licenses/by-nc/4.0/

[6] Dolan, James A. et al.: *Optical Properties of Gyroid Structured Materials: From Photonic Crystals to Metamaterials*, Advanced Optical Materials, 3, 12-32, 2015.

[7] Han Lu and Che Shunai: *An Overview of Materials with Triply Periodic Minimal Surfaces and Related Geometry: From Biological Structures to Self-Assembled Systems*, 30, 1705708, 2018.

[8] M. Saba et al.: *Absence of circular polarisation in reflections of butterfly wing scales with chiral gyroid structure*, Materials Today: Proceedings, 1, 193-208, 2014.

[9] A. Zubiri et al.: *Coexistence of both gyroid chiralities and individual butterfly wing scales of Callophyrs rubi*, Proceedings of the National Academy of Sciences, 112, 2015.

[10] *Britannica: lipid* https://www.britannica.com/science/lipid

[11] H. Ghiradella: *Structure and development of iridescent butterfly scales: Lattices and laminae*, Journal of Morphology, 202, 69-88, 1989.

[12] S. Salentinig et al.: *Self-assembled structures and pKa value of oleic acid in systems of biological relevance*, the ACS journal of surfaces and colloids, 26, 14, 2010.

[13] K. Kashmari et al.: *Optimal Molecular Dynamics System Size for Increased Precision and Efficiency for Epoxy Materials*, The Journal of Physical Chemistry B, 128, 4255-4265, 2024.

[14] R. Groot and P. Warren: *Dissipative particle dynamics: Bridging the gap between atomistic and mesoscopic simulation*, The Journal of Chemical Physics, 107, 1997.

[15] C. William et al.: *A computer simulation method for the calculation of equilibrium constants for the formation of physical clusters of molecules: Application to small water clusters*, J. Chem Phys, 1, 637-649, 1982.

[16] H. Doi et al.: *DPD simulation to reproduce lipid membrane microdomains based on fragment molecular orbital calculations*, Appl. Phys. Express, 17, 055001, 2024.

[17] *J-OCTA*
https://www.j-octa.com/cases/caseA61/

[18] D. W. Van Krevelen, K. Te Nijehuis: *Properties of polymers*, Elsevier, 4th edition, Netherlands 2009.

[19] M. Rubinstein and R. H. Colby: *Polymer Physics*, Oxford University Press, 1st edition, 2003.

[20] A. Khedr and A. Striolo: *DPD Parameters for Simultaneously Simulating Water-Oil Interfaces and Aqueous Nonionic Surfactants*, J. Chem. Theory Comput., 14, 12, 6460-6471, 2018.

[21] N. Arai et al.: *Self-assembly behaviours of primitive and modern lipid membrane solutions: a coarse-grained molecular simulation study*, Phys. Chem. Chem. Phys., 18, 19426-19432, 2016.

[22] A. L. Liu: *Advances in Planar Lipid Bilayers and Liposomes*, Academic Press, 1st edition, 2006.

[23] Michael Seaton: *DL_MESO_DPD: development and use of mesoscale modelling software*, Molecular Simulation, 47, 228-247, 2021.

[24] *SciPy documentation*
URL: https://docs.scipy.org/doc/scipy/index.html